

Red-Emissive Nanocrystals of $\text{Cs}_4\text{Mn}_x\text{Cd}_{1-x}\text{Sb}_2\text{Cl}_{12}$ Layered Perovskite

Emanuela Sartori,^{1,2} Marta Campolucci,^{1,2} Dmitry Baranov,² Min Zeng,^{3,4} Stefano Toso,^{2,5} Maurizio Ferretti,¹ Zeger Hens,⁴ Liberato Manna,² Federico Locardi^{1,2,4,*}

1 Department of Chemistry and Industrial Chemistry, Università degli Studi di Genova, Via Dodecaneso 31, 16146 Genova, Italy

2 Nanochemistry Department, Istituto Italiano di Tecnologia, Via Morego 30, 16163, Italy

3 Hubei Key Laboratory of Ferro- & Piezoelectric Materials and Devices, Faculty of Physics and Electronic Science, Hubei University, Wuhan, 430062, P. R. China

4 Physics and Chemistry of Nanostructures group (PCN), Ghent University, Krijgslaan 281, Gent 9000, Belgium

5 International Doctoral Program in Science, Università Cattolica del Sacro Cuore, 25121 Brescia, Italy

Abstract.

Layered double perovskite are currently investigated as emerging halide-based materials for optoelectronic applications. Herein, we present the synthesis of $\text{Cs}_4\text{Mn}_x\text{Cd}_{1-x}\text{Sb}_2\text{Cl}_{12}$ ($0 \leq x \leq 1$) nanocrystals (NCs). X-ray powder diffraction evidences the retaining of the same crystal structure for all the inspected composition; transmission electron microscopy revealed monodisperse particles with a mean size of 10.6 nm. The absorption spectra seem to be mostly determined by transitions related to Sb^{3+} , whereas Mn^{2+} induced a red emission in the 625 – 650 nm range. The emission intensity and position varies with the Mn^{2+} content and reaches the maximum for the composition with $x = 0.12$. Finally, we demonstrated that the photoluminescence quantum yield (PLQY) of the latter NCs was boosted from 0.3% to 3.9% through a post-synthesis treatment. The present work enlarges the knowledge of colloidal layered double perovskite nanocrystals, stimulating future investigations of this emerging class of material.

1. Introduction.

In recent years, the extensive research on lead halide perovskites¹ led to an increasing interest in new metal halides with a wide variety of structure and composition based on different transition metals.² In particular, the concerns about toxicity and limited stability inspired researchers to explore alternatives with comparable or better optoelectronic properties.^{3,4} Double perovskites (DPs) represent one of the first attempts of lead substitution. In DPs, the original 3D structure of lead halides, *i.e.* a framework composed of corner sharing $[\text{PbX}_6]$ ($\text{X} = \text{Cl}^-, \text{Br}^-, \text{I}^-$) octahedra, is retained by the alteration of octahedra formed by monovalent and trivalent cations.⁵ In this way, charge neutrality is maintained, as expressed through the general chemical formula $\text{A}_2\text{M}^+\text{M}^{3+}\text{X}_6$ ($\text{M} = \text{metal}$, $\text{X} = \text{Cl}^-, \text{Br}^-, \text{I}^-$). Several combinations of B^+ and B^{3+} cations have been tested, both in bulk and in nanocrystals (NCs), for example $\text{M}^+ = \text{Ag}^+$, Na^+ , K^+ and $\text{M}^{3+} = \text{In}^{3+}$, Bi^{3+} , Sb^{3+} .⁶⁻¹² In this kind of structure, due to the charge balance and the size matching, the introduction of bivalent metal cations (M^{2+}) is generally possible only in a low concentration.¹²⁻¹⁴

A complete substitution of the M^+ with a M^{2+} is possible with the contemporary introduction of a vacancy (Vac), resulting in a general $A_4M^{2+}M^{3+}_2X_{12}$ stoichiometry; these materials, due to their peculiar structure, are commonly known as $\langle 111 \rangle$ oriented layered double perovskites (LDPs).² Indeed, the structure can be described as a cubic sublattice of Cs^+ cations¹⁵ filled alternatively by layers of corner sharing $[M^{2+}X_6] - [M^{3+}X_6] - [M^{2+}X_6] - [VacX_6]$ octahedra along the $\langle 111 \rangle$ direction. The first LDP, $Cs_4CuSb_2Cl_{12}$, was synthesized as a bulk material by Solis-Ibarra's group in 2017 and showed an optical bandgap of 1 eV, which is promising for photovoltaics;¹⁶ Tong Cai *et al.* prepared the same composition as NCs, with optical properties in line with those of the corresponding powders.¹⁷ The partial substitution of Cu^{2+} with Mn^{2+} tunes the band gap to higher energy, and a low-intensity red emission was measured for $Cs_4MnSb_2Cl_{12}$.¹⁸ A more efficient emission has been observed with the partial introduction of Cd^{2+} , leading to a photoluminescence quantum yield (PLQY) of 28.5% for $Cs_4Cd_{0.8}Mn_{0.2}Sb_2Cl_{12}$.¹⁹ The replacement of Sb^{3+} with Bi^{3+} resulted in an increase of the PLQY²⁰ up to 79.5% for the composition $Cs_4Cd_{1-x}Mn_xBi_2Cl_{12}$ ($x=0.1$).²¹ H. Yang *et al.* successfully synthesized the same stoichiometry series in the form of nanocrystals; however, the resulting materials showed a 20-fold drop of the PLQY (4.6%) compared to bulk crystals.²² Very recently, the $Cs_4Cd_{1-x}Cu_xSb_2Cl_{12}$ system has been studied and tested as a potential candidate for photodetection.²³

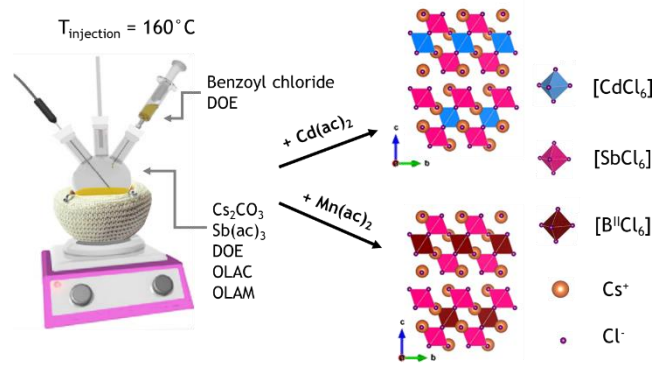
Motivated by the aforementioned studies, we explored the possibility to synthesize $Cs_4Cd_{1-x}Mn_xSb_2Cl_{12}$ in the form of NCs. Using a hot injection approach, we found that alloying Cd^{2+} and Mn^{2+} is possible in the whole x range ($x = Mn^{2+}$ fraction, $0 \rightarrow 1$) with the formation of phase-pure cuboidal nanoparticles. The optical characterization has revealed a red emission centered at 620-630 nm for all the samples except for $x = 0$, with the emission position and intensity depending on the Mn^{2+} amount. The sample with $x = 0.115$ yielded the most intense emission in the series, with a PLQY of 0.3% that was further enhanced ten-fold to 3.9% by means of a surface treatment with ammonium thiocyanate. Overall, our work expands the knowledge of the layered double perovskite at the nanoscale, evidencing the potential of these compounds as photoluminescent materials.

2. Results and Discussion.

We prepared $Cs_4Mn_xCd_{1-x}Sb_2Cl_{12}$ NCs through a hot-injection method. Briefly, the synthesis consisted of degassing the precursors (metal acetates and carbonates) under vacuum in mixture of dioctyl ether, oleylamine and oleic acid for 20 minutes at 115 °C, followed by an injection of benzoyl chloride at 160 °C under N_2 atmosphere (Scheme 1; see Supporting Information for details). The resulting nanoparticles had a cuboidal shape for all the inspected samples, with a Mn^{2+} content tunable by systematically changing the $Mn^{2+}/(Cd^{2+} + Mn^{2+})$ precursors ratio from 0 to 1. The ICP-OES analysis revealed that, in general, less Mn^{2+} than the loaded amount enters the structure, especially when the

$\text{Mn}^{2+}/(\text{Cd}^{2+} + \text{Mn}^{2+})$ ratio of the precursors is lower than 0.5 (Table S1 and Figure S1); a similar phenomenon was observed in $\text{Cs}_4\text{Mn}_x\text{Cd}_{1-x}\text{Bi}_2\text{Cl}_{12}$.²⁰

Scheme 1. Colloidal synthesis of $\text{Cs}_2\text{Mn}_x\text{Cd}_{1-x}\text{Sb}_2\text{Cl}_{12}$ ($0 \leq x \leq 1$) NC samples.



The analysis of the powder X-ray diffraction (XRD) data indicates that all the synthesized compositions crystallize in the same trigonal $R\bar{3}m$ structure (Figure 1a and S2) and the samples with intermediate x are pure and isostructural to the terminal compositions ($x = 0$ and 1, Figure 1b and S2), without the presence of secondary phases. The shape of nanocrystals reflects the influence of the cuboidal Cs^+ sublattice found in the structure, as commonly observed for other metal-halide perovskite nanocrystals.¹⁵ The slight shift of the diffraction peaks toward higher 2θ angles (Figure 1b inset) originates from the contraction of the unit cell due to the substitution of the smaller Mn^{2+} cation in the Cd^{2+} sites. Indeed, the cells parameters shifts from $a = 7.586$, $c = 37.165$ to $a = 7.549$, $c = 36.994$ for 0% Mn^{2+} and 100% Mn^{2+} , respectively. The unit cell contracts by -1.44% in volume, and the contraction was found to be isotropic ($a = -0.49\%$; $c = -0.46\%$), suggesting a random $\text{Mn}^{2+}/\text{Cd}^{2+}$ replacement in the structure (Figure S3). These results agree with the data reported on the corresponding powders.¹⁹ Transmission electron microscopy (TEM) micrographs of $\text{Cs}_4\text{Mn}_x\text{Cd}_{1-x}\text{Sb}_2\text{Cl}_{12}$ NCs evidenced the formation of NCs with a cuboidal shape (Figure 1c-e) and a mean size of ~ 10.6 nm when employing an amount of Mn^{2+} up to 80% ($x = 0.8$). For the larger Mn^{2+} fractions ($x = 0.9, 1$) we observed a smoothening of the cuboidal edges (Figures 1e and S4). Upon changing the injection temperature (*i.e.* 140 – 150 – 170 °C), we observed no changes in the crystal structure (Figure S5a), yet higher temperatures led to NC samples with a more polydisperse distribution of size and morphology (Figure S5b-e).

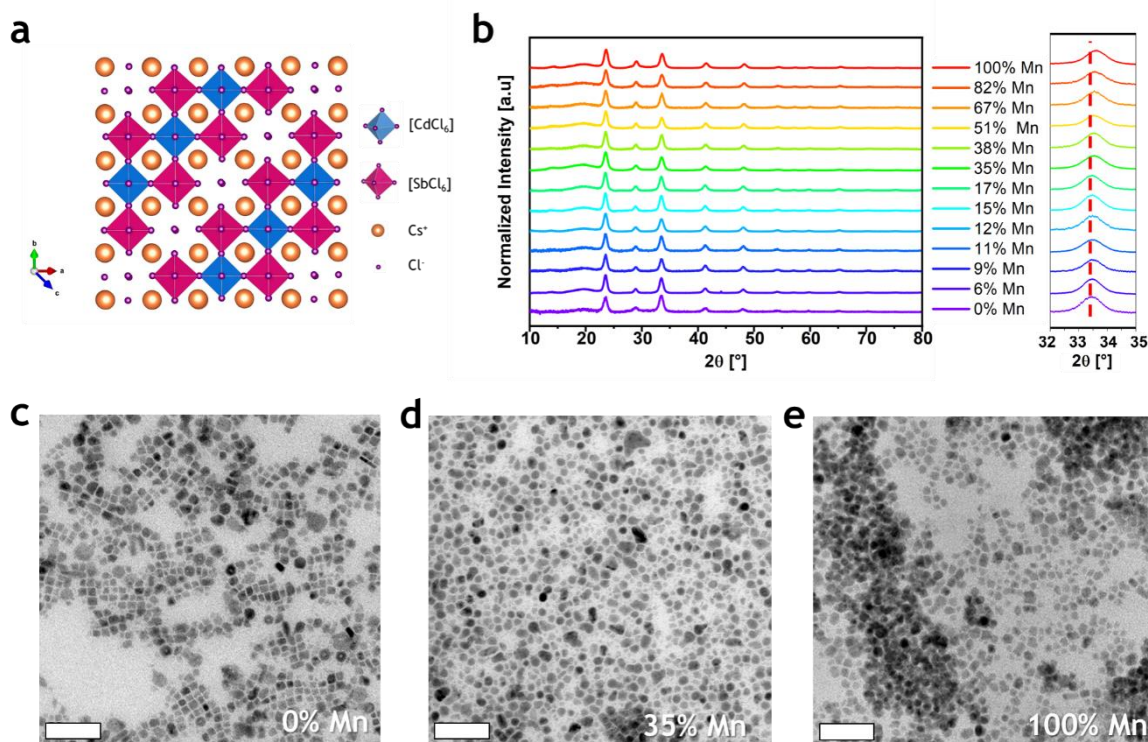


Figure 1. (a) Crystal structure of $\text{Cs}_4\text{CdSb}_2\text{Cl}_{12}$; (b) XRD patterns of $\text{Cs}_4\text{Mn}_x\text{Cd}_{1-x}\text{Sb}_2\text{Cl}_{12}$ NCs; a shift to higher angles increasing the Mn^{2+} amount was observed (inset); (c–e) TEM micrographs of $\text{Cs}_4\text{Mn}_x\text{Cd}_{1-x}\text{Sb}_2\text{Cl}_{12}$ NCs. Scalebars are 100 nm.

All samples display an absorption spectrum characterized by three different features: two broad peaks between 300 nm and 400 nm (Figure 2a and S6a) that are independent on the $\text{Mn}^{2+}/(\text{Cd}^{2+} + \text{Mn}^{2+})$ ratio, and a well-defined peak at 267 nm (for $x = 0$) whose intensity decreases with a contemporary blue shift with the increasing Mn^{2+} amount (Figure S6a). The observed behavior is consistent with the corresponding bulk material except for the intensity variation and shift of the last feature (250 – 300 nm), that was not previously observed by the Solis – Ibarra’s group.¹⁹ Overall, the absorption spectrum of $\text{Cs}_4\text{Mn}_x\text{Cd}_{1-x}\text{Sb}_2\text{Cl}_{12}$ seems to be mostly determined by transitions related to Sb^{3+} , not unlike previous observations on $\text{Cs}_3\text{Sb}_2\text{Cl}_9$.²⁴ Sb^{3+} is a ns^2 ion characterized by the $^1\text{S}_0$ ground state and four higher-energy levels denoted as $^3\text{P}_0$, $^3\text{P}_1$, $^3\text{P}_2$ and $^1\text{P}_1$.²⁵ The absorption in the 300 – 400 nm span can be ascribed to the partially allowed $^1\text{S}_0 \rightarrow ^3\text{P}_1$ transition, commonly named as the A band, split into a doublet; similarly, the allowed $^1\text{S}_0 \rightarrow ^1\text{P}_1$ transition (C – band) is responsible for the absorption signal found at ~ 270 nm.^{11,19,25} Instead, the $d \rightarrow d$ Mn^{2+} transition, generally observed for Mn–based materials between 400 nm and 550 nm, was not detected.

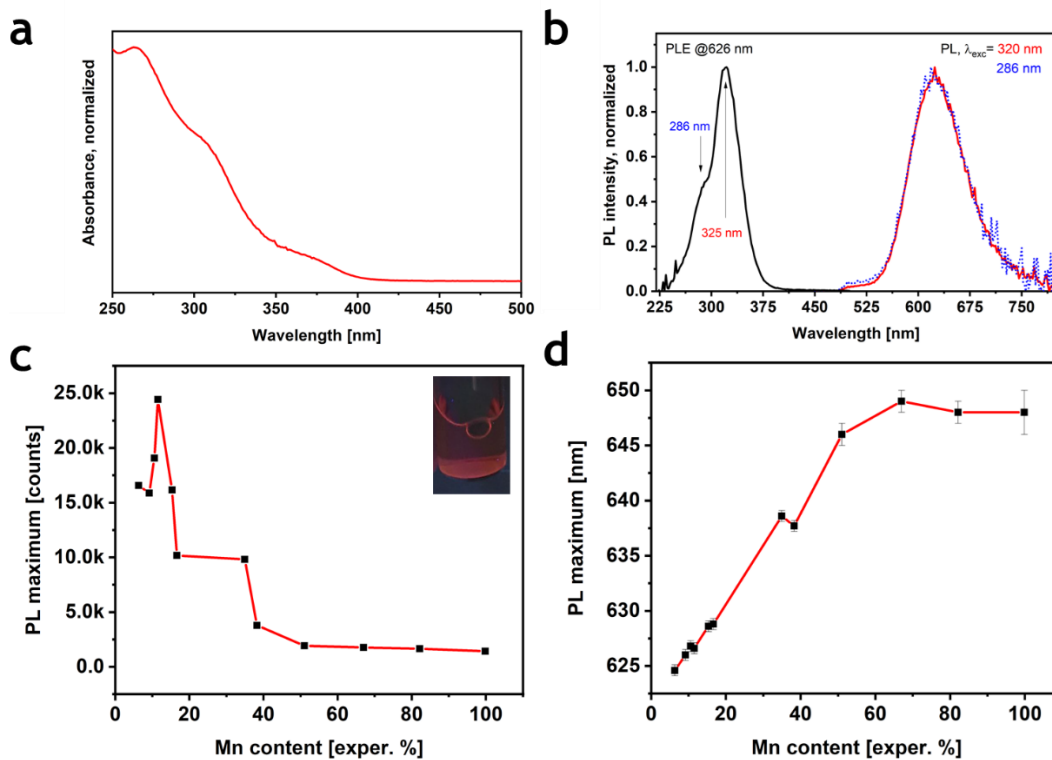


Figure 2. (a) Normalized optical absorption at 250 nm and (b) PLE and PL at two different excitation wavelengths (320 nm and 286 nm) of $\text{Cs}_4\text{Mn}_{0.12}\text{Cd}_{0.88}\text{Sb}_2\text{Cl}_{12}$ chosen as representative. (c) PL intensity (normalized at the absorption at 320 nm) behavior at increasing Mn^{2+} content, the inset shows a photograph of the most emissive sample under UV light. (d) position of the PL peak at increasing Mn^{2+} content.

All the $\text{Cs}_4\text{Mn}_x\text{Cd}_{1-x}\text{Sb}_2\text{Cl}_{12}$ compositions, except for $x = 0$, show a red emission centered at around 620-650 nm under UV excitation (Figure S6b). The photoluminescence excitation (PLE) shape spectra exhibit an intense peak centered at ~325 nm with a shoulder at ~285 nm (Figure 2b). The PLE behavior resembles that of absorption, indicating that the excitation occurs through the Sb^{3+} bands. Interestingly, even if Sb^{3+} is known for having optical emission in metal halides,^{25,26} we did not detect any PL signal in $\text{Cs}_4\text{CdSb}_2\text{Cl}_{12}$, whereas the ${}^4\text{T}_1 \rightarrow {}^6\text{A}_1$ transition of Mn^{2+} induced the red emission in all the other samples. We explain this behavior by an energy transfer between antimony(III) and manganese(II) ions, $\text{Sb}^{3+} \rightarrow \text{Mn}^{2+}$.²⁷ Indeed, the PLE profiles are the same for all the samples without considerable shifting (Figure S6c), while significant differences were detected both in the PL intensity and positions (Figure 2c-d and S6b). No differences in the PL were observed when exciting at a different wavelength (Figure 2b). The intensity increases with the Mn^{2+} ratio (Figure 2c) up to a maximum at the experimental composition of 11.5% Mn^{2+} . Similar results were reported for the corresponding bulk system.¹⁹ However, we observed a red shift of the PL peak related to the increasing amount of Mn^{2+} (Figure 2d). With increasing Mn^{2+} concentration the emission gradually shifts from 624 nm (6% Mn^{2+}), a value higher than in bulk $\text{Cs}_4\text{Mn}_x\text{Cd}_{1-x}\text{Sb}_2\text{Cl}_{12}$ but close to reports for the Bi-based counterpart $\text{Cs}_2\text{MnBi}_2\text{Cl}_{12}$,^{20,22} to a roughly constant spectral position of ~648 nm for $x > 0.5$. The Mn^{2+} emission

shift was already reported in $\text{Cs}_4\text{Mn}(\text{Bi}_{1-x}\text{In}_x)_2\text{Cl}_{12}$ ²⁸ and CsPbCl_3 ,^{29,30} and ascribed to a contraction of the unit cell. According to the Tanabe-Sugano diagram for the d^5 ion (*e.g.* Mn^{2+}), an increase of the crystal field induces a red shift in the ${}^4\text{T}_1 \rightarrow {}^6\text{A}_1$ transition. Indeed, it is reasonable that the progressive substitution of Cd^{2+} with the smaller Mn^{2+} shrinks the volume of the $[\text{MnCl}_6]$ octahedra,¹⁹ thus inducing the observed red shift. The variation of the PL intensity can be instead explained considering that the maximum intensity is reached, in principle, when the MnCl_6 octahedra are completely surrounded by $[\text{SbCl}_6]$ and $[\text{CdCl}_6]$ octahedra, thus, avoiding any Mn – Mn self – quenching.

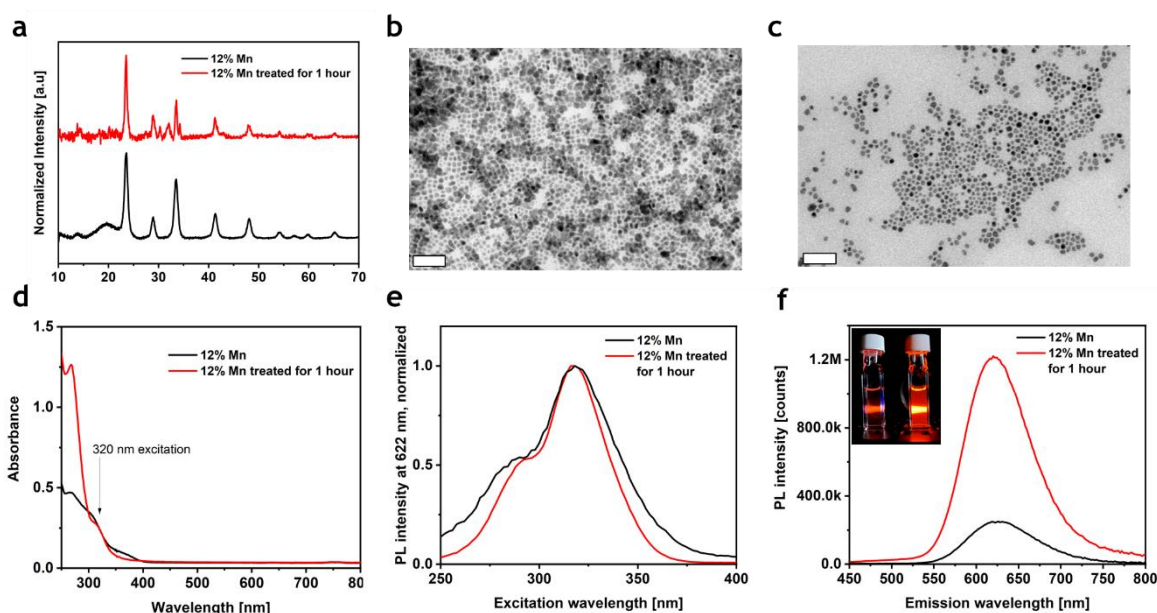


Figure 3. (a) XRD of $\text{Cs}_4\text{Mn}_{0.12}\text{Cd}_{0.88}\text{Sb}_2\text{Cl}_{12}$ before (black line) and after thiocyanate treatment (red line). (b) and (c) TEM images before and after the thiocyanate treatment, respectively. (d) ABS, (e) PLE, (f) PL of $\text{Cs}_4\text{Mn}_{0.12}\text{Cd}_{0.88}\text{Sb}_2\text{Cl}_{12}$ before (black line) and after thiocyanate treatment (red line). Inset in (f) shows a photograph under UV lamp of the sample with (bright orange) and without the treatment (dark orange).

The PLQY of the most emissive colloidal sample was measured to be 0.3%, a value that is much lower than that reported for the corresponding bulk material (28.5%).¹⁹ The decrease of PLQY upon reduced particle size has been previously detected in $\text{Cs}_4\text{Mn}_x\text{Cd}_{1-x}\text{Bi}_2\text{Cl}_{12}$: when lowering the dimensions of the particles from micrometers to nanometers, the PLQY collapses from 79.5%²¹ to 4.6%.²² This unfavorable effect, already documented in several metal-halide perovskites, can be ascribed to the formation of non-radiative relaxation paths induced by surface traps. To test this hypothesis, we attempted three different post-synthetic treatments to boost the PLQY of the nanocrystals: a small fraction of the nanocrystals suspension was added to i) a mixture of CdCl_2 , OA and OIAm in hexane;^{29,31} ii) a solution of didodecyldimethylammonium chloride (DDAC) in toluene;³² iii) a mixture of ammonium thiocyanate (NH_4SCN) in hexane^{33,34} (see Experimental parts). The first two treatments decomposed the samples, while the emission was successfully enhanced by NH_4SCN . During the treatment, the sample emission kept increasing for one hour (Figure S7a), after which it started

decreasing due to the progressive decomposition of the sample, that completely evolved in other phases after three hours (Figure S7b). The XRD and TEM analyses on the brightest sample (Figure 3a) showed that the crystalline phase was preserved, even if a small amount of a secondary phase, identified as CsCl, was present. By TEM, the morphology of the NCs had been largely preserved, but cuboidal shapes appeared more rounded with respect to the pristine sample (Figure 3b-c). The absorption spectrum revealed a small decrease in the 350 – 400 nm span and an enhancement of the C – band ($\lambda < 300$ nm) (Figure 3d). Furthermore, the PLE spectrum narrowed without significant shift (Figure 3e). More importantly, an enhanced PL emission was observed, that resembled the same broadness of the pristine material with a small shift of ~ 2 nm (Figure 3f and S8). The conservation of the PLE and PL spectral shapes and positions suggests that the post treatment does not influence the environment around Mn^{2+} (*i.e.*, the crystal structure), but reduces the number of non-radiative relaxation channels, likely by passivating the surface sites. Indeed, the PLQY reached a value of 3.9% (Figure S9) that is 10 times higher with respect to the as-synthesized particles, and comparable to the Bi – based counterpart.

3. Conclusions.

In summary, we successfully synthesized $\text{Cs}_4\text{Mn}_x\text{Cd}_{1-x}\text{Sb}_2\text{Cl}_{12}$ nanocrystals with a tunable composition in the $x = 0 - 1$ range. All the sample showed an UV absorption and a red emission from Sb^{3+} and Mn^{2+} ions (except for the Mn-free $x = 0$), respectively. The PL intensity changed with the Mn^{2+} amount, reaching a maximum for $x = 0.12$. The pristine sample featured a low PLQY ($< 1\%$) that was boosted to 3.9% by a post-synthesis treatment with ammonium thiocyanate. The intriguing optical properties of $\text{Cs}_4\text{Mn}_x\text{Cd}_{1-x}\text{Sb}_2\text{Cl}_{12}$ nanocrystals should stimulate additional studies on this emerging family of layered double perovskites.

Conflicts of interest. Authors declares no conflicts of interest

Acknowledgements. The authors thank Materials Characterization Facility and Electron Microscopy Facility at the Fondazione Istituto Italiano di Tecnologia for use of XRD and TEM equipment and technical support, Filippo Drago of Nanochemistry Facility for elemental analysis using ICP-OES. Z.H acknowledges Ghent University (GOA 01G01019) and FWO-Vlaanderen (SBO Proceed) for research funding.

References

- 1 Q. A. Akkerman, G. Rainò, M. V. Kovalenko and L. Manna, *Nat. Mater.*, 2018, **17**, 1–12.
- 2 B. Vargas, G. Rodríguez-López and D. Solis-Ibarra, *ACS Energy Lett.*, 2020, **5**, 3591–3608.
- 3 W. Ke and M. G. Kanatzidis, *Nat. Commun.*, 2019, **10**, 1–4.
- 4 X. Li, X. Gao, X. Zhang, X. Shen, M. Lu, J. Wu, Z. Shi, V. L. Colvin, J. Hu, X. Bai, W. W. Yu and Y. Zhang, *Adv. Sci.*, 2021, **8**, 1–33.
- 5 F. Giustino and H. J. Snaith, *ACS Energy Lett.*, 2016, **1**, 1233–1240.
- 6 J. Luo, X. Wang, S. Li, J. Liu, Y. Guo, G. Niu, L. Yao, Y. Fu, L. Gao, Q. Dong, C. Zhao, M. Leng, F. Ma, W. Liang, L. Wang, S. Jin, J. Han, L. Zhang, J. Etheridge, J. Wang, Y. Yan, E. H. Sargent and J. Tang, *Nature*, 2018, **563**, 541–545.
- 7 F. Locardi, E. Sartori, J. Buha, J. Zito, M. Prato, V. Pinchetti, M. L. Zaffalon, M. Ferretti, S. Brovelli, I. Infante, L. De Trizio and L. Manna, *ACS Energy Lett.*, 2019, **4**, 1976–1982.
- 8 N. R. Wolf, B. A. Connor, A. H. Slavney and H. I. Karunadasa, *Angew. Chemie - Int. Ed.*, 2021, **60**, 16264–16278.
- 9 G. Volonakis, A. A. Haghighirad, R. L. Milot, W. H. Sio, M. R. Filip, B. Wenger, M. B. Johnston, L. M. Herz, H. J. Snaith and F. Giustino, *J. Phys. Chem. Lett.*, 2017, **8**, 772–778.
- 10 S. E. Creutz, E. N. Crites, M. C. De Siena and D. R. Gamelin, *Nano Lett.*, 2018, **18**, 1118–1123.
- 11 A. Nocolak, A. Nocolak, V. Morad, V. Morad, K. M. McCall, S. Yakunin, Y. Shynkarenko, S. Yakunin, Y. Shynkarenko, M. Wörle and M. V. Kovalenko, *Chem. Mater.*, 2020, **32**, 5118–5124.
- 12 F. Locardi, M. Cirignano, D. Baranov, Z. Dang, M. Prato, F. Drago, M. Ferretti, V. Pinchetti, M. Fanciulli, S. Brovelli, L. De Trizio and L. Manna, *J. Am. Chem. Soc.*, 2018, **140**, 12989–12995.
- 13 Q. Liao, J. Chen, L. Zhou, T. Wei, L. Zhang, D. Chen, F. Huang, Q. Pang and J. Z. Zhang, *J. Phys. Chem. Lett.*, 2020, **11**, 8392–8398.
- 14 N. K. Nila and N. Angshuman, *Chem. Commun.*, 2018, **54**, 5205–5208.
- 15 S. Toso, D. Baranov and L. Manna, *ACS Energy Lett.*, 2020, **5**, 3409–3414.
- 16 B. Vargas, E. Ramos, E. Pérez-Gutiérrez, J. C. Alonso and D. Solis-Ibarra, *J. Am. Chem. Soc.*, 2017, **139**, 9116–9119.
- 17 T. Cai, W. Shi, S. Hwang, K. Kobbekaduwa, Y. Nagaoka, H. Yang, K. Hills-Kimball, H. Zhu, J. Wang, Z. Wang, Y. Liu, D. Su, J. Gao and O. Chen, *J. Am. Chem. Soc.*, 2020, **142**, 11927–11936.
- 18 B. Vargas, R. Torres-Cadena, J. Rodríguez-Hernández, M. Gembicky, H. Xie, J. Jiménez-Mier, Y. S. Liu, E. Menéndez-Proupin, K. R. Dunbar, N. Lopez, P. Olalde-Velasco and D. Solis-Ibarra, *Chem. Mater.*, 2018, **30**, 5315–5321.
- 19 B. Vargas, E. Coutiño-Gonzalez, O. Ovalle-Encinia, C. Sánchez-Aké and D. Solis-Ibarra, *J. Phys. Chem. Lett.*, 2020, **11**, 10362–10367.
- 20 N. P. Holzapfel, J. D. Majher, T. A. Strom, C. E. Moore and P. M. Woodward, *Chem. Mater.*, 2020, **32**, 3510–3516.
- 21 B. Vargas, D. T. Reyes-Castillo, E. Coutino-Gonzalez, C. Sánchez-Aké, C. Ramos, C. Falcony and D. Solis-Ibarra, *Chem. Mater.*, 2020, **32**, 9307–9315.
- 22 H. Yang, W. Shi, T. Cai, K. Hills-Kimball, Z. Liu, L. Dube and O. Chen, *Nanoscale*, 2020, **12**, 23191–23199.
- 23 T. Cai, W. Shi, D. J. Gosztol, K. Kobbekaduwa, H. Yang, N. Jin, Y. Nagaoka, L. Dube, J. Schneider, S. Hwang, J. Gao, X. Ma and O. Chen, *Matter*, 2021, **4**, 2936–295.
- 24 B. Pradhan, G. S. Kumar, S. Sain, A. Dalui, U. K. Ghorai, S. K. Pradhan and S. Acharya, *Chem. Mater.*, 2018, **30**, 2135–2142.
- 25 Y. Jing, Y. Liu, M. Li and Z. Xia, *Adv. Opt. Mater.*, 2021, **9**, 1–15.
- 26 H. Arfin, A. S. Kshirsagar, J. Kaur, B. Mondal, Z. Xia, S. Chakraborty and A. Nag, *Chem. Mater.*, 2020, **32**, 10255–10267.
- 27 X. Liu, X. Xu, B. Li, L. Yang, Q. Li, H. Jiang and D. Xu, *Small*, 2020, **16**, 1–7.
- 28 S. He, S. Fang, T. Han, T. Lang, M. Cai, H. You, L. Peng, S. Cao, B. Liu, Q. Qiang, J. Chen and B. Lei, *J. Phys. Chem. C*, 2021, **125**, 31, 16938–16945.
- 29 S. Ji, X. Yuan, S. Cao, W. Ji, H. Zhang, Y. Wang, H. Li, J. Zhao and B. Zou, *J. Phys. Chem.*

- Lett.*, 2020, **11**, 2142–2149.
- 30 H. Liu, Z. Wu, J. Shao, D. Yao, H. Gao, Y. Liu, W. Yu, H. Zhang and B. Yang, *ACS Nano*, 2017, **11**, 2239–2247.
- 31 N. Mondal, A. De and A. Samanta, *ACS Energy Lett.*, 2019, **4**, 32–39.
- 32 M. Imran, J. Ramade, F. Di Stasio, M. De Franco, J. Buha, S. Van Aert, L. Goldoni, S. Lauciello, M. Prato, I. Infante, S. Bals and L. Manna, *Chem. Mater.*, 2020, **32**, 10641–10652.
- 33 M. Lu, J. Guo, P. Lu, L. Zhang, Y. Zhang, Q. Dai, Y. Hu, V. L. Colvin and W. W. Yu, *J. Phys. Chem. C*, 2019, **123**, 22787–22792.
- 34 V. G. V. Dutt, S. Akhil and N. Mishra, *ChemNanoMat*, 2020, **6**, 1730–1742.